Available online at www.sciencedirect.com
SCIENCE DIRECT®
Journal of Solid State Chemistry 178 (2005) 2715–2723
JOURNAL OF SOLID STATE CHEMISTRY
www.elsevier.com/locate/jssc

High-temperature thermodynamic and transport properties of the $Sr_3Fe_2O_{6+\delta}$ mixed conductor

L. Mogni[a], J. Fouletier[b], F. Prado[a], A. Caneiro[a,*]

[a]Centro Atómico Bariloche, CNEA, Instituto Balseiro, Unidad de Achividad Technologia, 8400 S. C. de Bariloche RN, Argentina
[b]Laboratoire d'Electrochimie et de Physicochimie des Matériaux et des Interfaces (L.E.P.M.I), E.N.S.E.E.G., I. N. P. Grenoble, BP 75, 38402 Saint Martin d'Heres, Cedex, France

Received 11 April 2005; received in revised form 27 May 2005; accepted 13 June 2005
Available online 20 July 2005

Abstract

We report a systematic study of the non-stoichiometry and high-temperature transport properties of the perovskite related mixed conductor $Sr_3Fe_2O_{6+\delta}$. The variation of the oxygen content $(6+\delta)$ with T and equilibrium oxygen partial pressure (pO_2) was obtained by thermogravimetry within the range: $10^{-5} < pO_2 < 1$ atm.; $400 \leqslant T \leqslant 1100\,^{\circ}C$. From the experimental values of the oxygen chemical potential (μ_{O_2}), the partial molar enthalpy (h_{O_2}) and the partial molar entropy (s_{O_2}) were determined for the composition range $6.00 < 6+\delta < 6.55$. A simple defect model based on the mass action law assuming localized charge carriers and oxygen vacancies was used to reproduce the thermodynamic data.

Electrical resistivity measurements as a function of pO_2 at constant temperature were obtained within the interval $650 \leqslant T \leqslant 1000\,^{\circ}C$. The activation energy values for the electrical transport process at constant oxygen content values were obtained from the combination of electrical conductivity and thermogravimetry data. The electrical transport data are in agreement with the small polaron model.

Keywords: Mixed conductors; Ruddlesden–Popper phases; Thermodynamic properties; Partial molar properties; Defect structure; Electrical conductivity; Small polaron

1. Introduction

The search of new materials with mixed conductivity has focused in the last decade the attention of material scientists in view of its use as cathode materials for solid oxide fuel cells (SOFC), and oxygen separation membranes [1,2]. These applications require materials with a high thermodynamic stability, a high catalytic activity for oxygen dissociation and a thermal and chemical compatibility with solid electrolytes.

Manganites and cobaltites of La with perovskite structure have been extensively studied for using as cathodes in SOFC [3–6].

The La-manganites exhibit good thermal and chemical compatibility with YSZ (Yttria stabilized zirconia) solid electrolyte. However, they are not suitable to be used in SOFC that operates at intermediate temperatures $T \sim 700\,^{\circ}C$ (IT-SOFC) since its ionic conductivity decreases considerably with the consequent diminution of the rate of O_2 reduction. The La-cobaltites show better ionic conductivity properties than those of La-manganites, but they react with YSZ solid electrolytes at high temperatures.

Among the mixed conductors materials with perovskite structure, the Fe-cobaltites with formula $(La,Sr)(Co,Fe)O_{3-\delta}$ show high oxygen permeation properties and therefore fulfill the mixed conductivity condition required for electrochemical applications. In particular the cubic phase $SrFe_{0.2}Co_{0.8}O_{3-\delta}$ exhibits the

*Corresponding author. Fax: +54 2944 445299.
E-mail address: caneiro@cab.cnea.gov.ar (A. Caneiro).

0022-4596/$ - see front matter © 2005 Elsevier Inc. All rights reserved.
doi:10.1016/j.jssc.2005.06.010

highest ionic conductivity ($0.01 < \sigma_i < 1\,Scm^{-1}$) of these perovskites. Unfortunately, this material tends to loose oxygen and decompose under the operating conditions at high temperatures (900 °C) and reducing environments (N_2, CH_4). On the other hand, around $3-\delta \sim 2.5$ at $T < 800\,^{\circ}C$, it undergoes a structural transition to a brownmillerite phase with orthorhombic symmetry involving the ordering of oxygen vacancies. This transition affects the oxygen permeation properties and its mechanical integrity [7,8].

The layer compounds with perovskite related structure of general formula $A_{n+1}B_nO_{3n+1}$ ($A = La, Sr$, $B = Fe, Ni, Co$, and $n = 1, 2, 3$) can be also considered for electrochemical applications since the presence of mixed conductivity has been recently reported for some of them [9–11]. The so-called Ruddlesden–Popper (R–P) phases, show better thermodynamic stability that the Fe-cobaltites and they do not present any phase transition within the working temperature and oxygen partial pressure (pO_2) ranges used for electrochemical applications. The structure of these layered compounds consists of n perovskite layers alternating with rock salt blocks. The electronic properties of compounds belonging to each homologous series are different between them. Thus, for instance the Sr_2FeO_4 compound ($n = 1$), is semiconductor, while $SrFeO_3$ ($n = \infty$) is metallic and the $Sr_3Fe_2O_7$ ($n = 2$) show an intermediate behavior [12]. Particularly, the $n = 2$ series are easy to obtain as single-phase materials. Fig. 1 shows the crystal structure for the $A_3B_2O_7$ compound. The structural stability and the oxygen permeation properties of the $Sr_{3-x}La_xFe_{2-y}Co_yO_{6+\delta}$ compounds have been recently studied due to the existence of mixed conductivity properties. The values of the ionic conductivity σ_i reach values between 0.01 and $0.05\,Scm^{-1}$ and the electronic conductivity σ_e varies between 20 and 100 for the $(Sr, La)_3(Co, Fe)_2O_{6+\delta}$ compounds [10].

The knowledge of the thermodynamic stability and the defect structure at high temperatures and its relation with the transport properties are essential to evaluate the behavior of these materials for high-temperature electrochemical applications. Besides, the study of the effects of cation substitution on the starting material ($Sr_3Fe_2O_{6+\delta}$) requires a deep knowledge on their fundamental properties.

Recently, Patrakeev et al. [13] have reported the transport properties of the $Sr_3Fe_2O_{6+\delta}$ compound within a wide range of pO_2. The electrical conductivity for $\delta > 0$ is analyzed using a point defect model assuming the formation of localized electron–holes (Fe^{+4}). The electrical conductivity data are fitted with a $\sigma \propto pO_2^{1/4}$ dependence [13].

The aim of the present work was to study in detail the high-temperature thermodynamic properties and the electrical conductivity of the $Sr_3Fe_2O_{6+\delta}$ compound for $\delta > 0$, within the temperature range $400 < T < 1100\,^{\circ}C$ and $10^{-5} < pO_2 < 1$ atm. The thermodynamic study was carried out by equilibrium pO_2 measurement as a function of T and oxygen content $(6+\delta)$. From these data the partial molar properties s_{O_2} and h_{O_2} were evaluated. The dependence of both s_{O_2} and h_{O_2} vs. $6+\delta$ is discussed assuming a defect model involving the presence of random charge localized carriers and a random distribution of oxygen vacancies. The measurements of oxygen content as a function of T and pO_2 together with the electrical conductivity data allowed us to determine the activation energy for the conduction process and to confirm the presence of double charged oxygen vacancies. The electrical conductivity values are in agreement with the small polaron model.

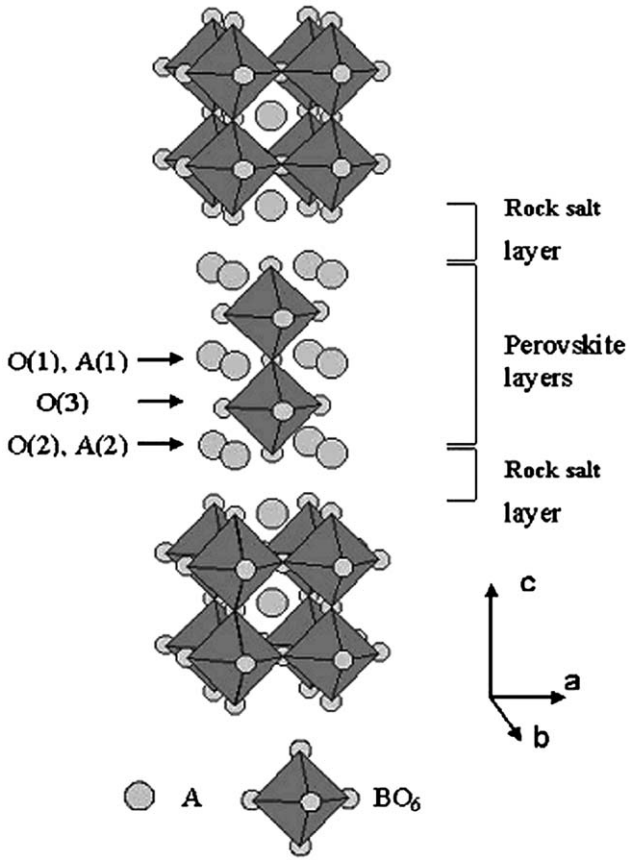

Fig. 1. Crystal structure of tetragonal $A_3B_2O_7$ (s.g. $I4/mmm$).

The data of the present work are compared with those of other perovskites such as $(La, Sr)(Fe, Co)O_{3-\delta}$ and $(La, Ca, Sr)CrO_{3-\delta}$ since their structures are related with the R–P phases and therefore a similar behavior should be expected [13–20].

2. Experimental

The $Sr_3Fe_2O_{6+\delta}$ sample was synthesized following an acetic-based gel route using high-purity Fe acetate (99.9% GFS Chemicals) and $SrCO_3$ (99.99% Alfa

Aesar) as raw materials [10]. The obtained gel was dried and decomposed at 450 °C for 30 min in air. An intermediate heat treatment was performed at 950 °C for 12 h in air. Dense samples were obtained by pressing the powders into pellets with a final heating treatment at 1300 °C under pure O_2 for 20 h with a cooling rate of 1 °C/min. The presence of single-phase materials was checked by XRD with a Philips PW1700 diffractometer using Cu$K\alpha$ radiation and a graphite monochromator. The diffractogram was refined by the Rietveld method in the $I4/mmm$ space group with lattice parameters $a = 3.8678$ (1) Å and $c = 20.173$ (1) Å. The homogeneity of the samples was confirmed by SEM observations and EDS analysis.

Isothermal measurements of the equilibrium pO_2 vs. oxygen content were performed using a highly sensitive thermogravimetry equipment [21] consisting of a symmetrical thermobalance based on a Cahn 1000 electrobalance coupled to an electrochemical gas blending system. This electrochemical system (zirconia pump and oxygen sensor) [22] provides a controlled Ar–O_2 atmosphere for the thermobalance with pO_2 values ranging from 10^{-6} to 1 atm. The thermobalance allows the determination of sample mass changes within ±10 μg, i.e. for our samples of about 0.6 g of $Sr_3Fe_2O_{6+\delta}$, were determined changes in $6+\delta$ within ±0.0003. The equilibrium criterion for the thermodynamic measurements was "constant sample weight with time, within ±10 μg". This equilibrium criterion was verified over a period of 24 h for the low T and pO_2 range of measurements. The oxygen content was determined by in situ reduction in dry H_2 at 1000 °C assuming SrO and Fe as final products. The equilibrium pO_2 isotherms were determined within the T and pO_2 range: $400 \leqslant T \leqslant 1100$ °C; $10^{-5} \leqslant pO_2 \leqslant 1$ atm.

DC resistivity measurements at high temperatures and controlled pO_2 were carried out by a standard four probe method on a rectangular sample of 1.5 mm × 5 mm × 20 mm.

3. Results and discussion

3.1. Thermodynamic measurements and partial molar properties

In Fig. 2 are plotted the equilibrium pO_2 isotherms as a function of the oxygen content "$6+\delta$". All isotherms were perfectly reproducible upon oxidation (reduction) and subsequent reduction (oxidation). Therefore, they must be considered stable equilibrium states of the $Sr_3Fe_2O_{6+\delta}$ compound. The equilibrium times were a few hours for the high T and pO_2 range and more than 2 days for low T and pO_2 values.

The equilibrium pO_2 data do not indicate any phase transition within our range of measurements. This is in agreement with a previous high-temperature XRD study under controlled pO_2 [10] performed within a T and pO_2 range similar to that of the present study.

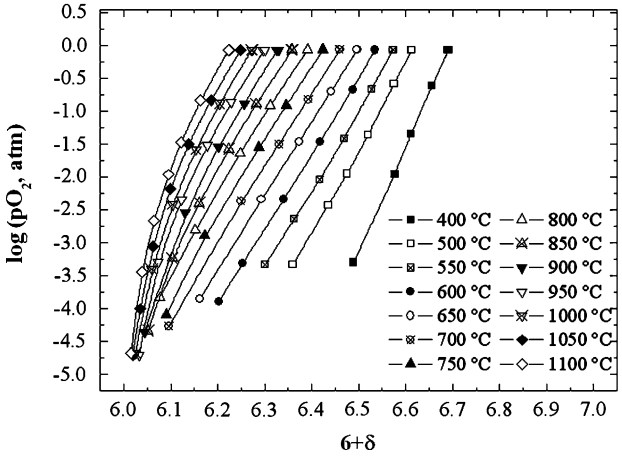

Fig. 2. Isotherms of log pO_2 vs. "$6+\delta$" for $Sr_3Fe_2O_{6+\delta}$ at several temperatures.

From the equilibrium pO_2 data shown in Fig. 2, the oxygen chemical potential of the gas and the oxide phase can be determined by the relation:

$$\mu_{O_2}^{oxide}(P,T) = \mu_{O_2}^{gas}(P,T) = \mu_{O_2}^{0}(T) + RT\ \ln(pO_2), \qquad (1)$$

where $\mu_{O_2}^{0}(T)$ is the reference state at 1 atm. (see Ref. [23]), R is the gas constant and T the temperature in K. The variation of $\mu_{O_2}^{oxide}(P,T)$ with the oxygen content at several temperatures is shown in Fig. 3. $\mu_{O_2}^{oxide}(P,T)$ is practically linear for high values of "$6+\delta$" and decreases more rapidly as the oxygen content approaches to 6. This rapid variation suggests an appreciable contribution of the configurational entropy to $\mu_{O_2}^{oxide}(P,T)$ due to the stabilization of the $Sr_3Fe_2O_6$ compound with all Fe as Fe^{3+}. For high values of "$6+\delta$" the more significant contribution to $\mu_{O_2}^{oxide}(P,T)$ is mainly due to the enthalpy term.

The partial molar properties s_{O_2} and h_{O_2} are defined through the thermodynamic relationship:

$$\mu_{O_2} = h_{O_2} - s_{O_2}T \qquad (2)$$

and can be computed from the data of Fig. 3 by the following expressions:

$$h_{O_2} = \left.\frac{\partial(\mu_{O_2}/T)}{\partial(1/T)}\right|_{\delta} \qquad (3)$$

and

$$s_{O_2} = -\left.\frac{\partial(\mu_{O_2})}{\partial(T)}\right|_{\delta}. \qquad (4)$$

In Figs. 4 and 5 are shown both s_{O_2} and h_{O_2} data as a function of the oxygen content "$6+\delta$", respectively. The s_{O_2} increases as $6+\delta$ decreases. For $\delta = 0$ and $\delta = 1$, the end-compounds $Sr_3Fe_2O_6$ and $Sr_3Fe_2O_7$ of the $Sr_3Fe_2O_{6+\delta}$ solid solutions are obtained.

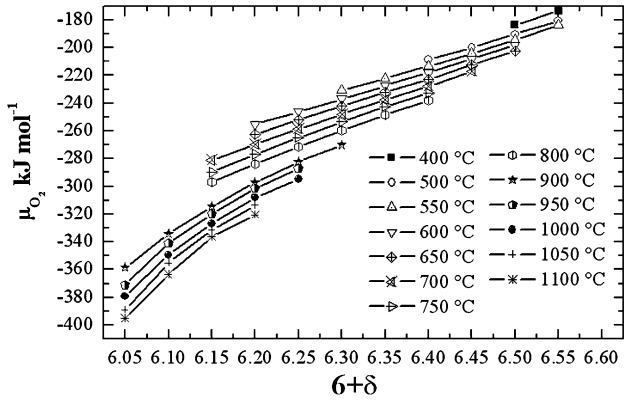

Fig. 3. Oxygen chemical potential for $Sr_3Fe_2O_{6+\delta}$ at several temperatures obtained from thermogravimetry data.

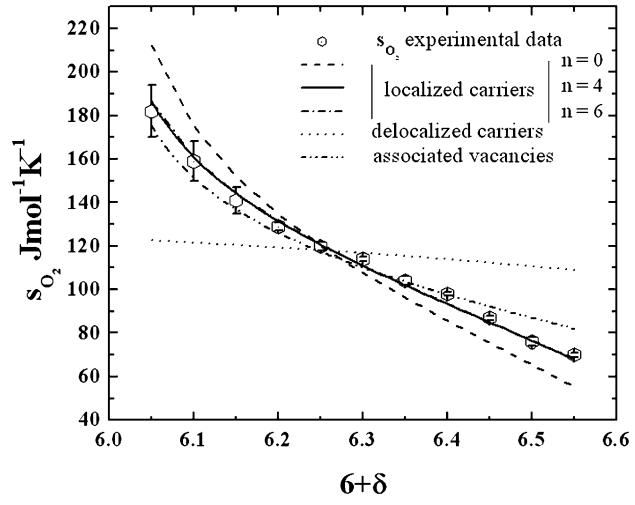

Fig. 4. Partial molar entropy, s_{O_2}, as a function of oxygen content "$6+\delta$".

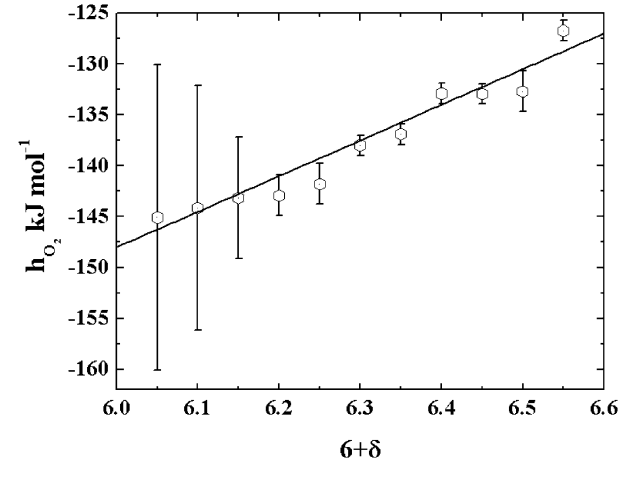

Fig. 5. Partial molar enthalpy, h_{O_2}, as a function of "$6+\delta$".

The mixing entropy of (S_{mix}) for the end-compounds ($\delta = 0$ and $\delta = 1$) must rapidly approach to zero with divergent slopes. Therefore, the partial molar entropy

$$s_{O_2} = \left.\frac{\partial S_{mix}}{\partial n_{O_2^{oxide}}}\right|_{T,P,n_i}$$

should diverge at $\delta = 0$ and 1. This is in agreement with the rapid increase of s_{O_2} in Fig. 4 as δ approaches zero, which indicates the presence of an ordered compound and that the main contribution to the entropy is of configurational nature. This behavior is similar to that reported for the $(La, Sr)(Fe, Co)O_{3-\delta}$ perovskites as $\delta \rightarrow 0$ [14–17].

The partial molar enthalpy h_{O_2} increases slowly with $6+\delta$. A similar behavior but with a higher slope has been observed for the $(La, Sr)(Fe, Co)O_{3-\delta}$ perovskites. For these compounds the variation of h_{O_2} with the oxygen content is attributed to the contribution of the delocalized carriers created in the Co band by the oxygen vacancy formation [14–16]. Recently, a point defect model considering localized charge carriers and defect interactions for the $(La, Ca)CrO_3$ perovskite has been reported [24]. In this case, the interactions between defects modify the standard enthalpy and therefore h_{O_2}. The non-ideality is included through the activity coefficients of each defect species.

The $(La, Sr)FeO_3$ material also presents localized charge carriers [13,16,17]. Recently, Patrakeev et al. [13] reports a similar behavior for the $Sr_3Fe_2O_{6+\delta}$ compound. Therefore, the existence of localized charge carriers in the $A_{n+1}B_nO_{3n+1}$ ($n = 1, 2, \infty$) perovskite related compounds seems to be associated to the presence of Fe in the *B* site. This assumption is confirmed in the present study by electrical resistivity measurements (see 3.3). Thus, we attribute the variation of the partial molar enthalpy as a function of "δ" to a deviation of the ideal solution model due to point defects interactions.

3.2. The defect model and the partial molar properties

In the $Sr_3Fe_2O_{6+\delta}$ compound, we consider that the oxygen non-stoichiometry, at high temperatures, is accommodated by filling the lattice oxygen vacancies sites available in the $Sr_3Fe_2O_6$ compound. We assume that $Sr_3Fe_2O_6$ is the stoichiometric composition of a highly acceptor-doped compound, which can be generated by doping with Sr an undoped stoichiometric reference compound such as $SrLa_2Fe_2O_7$ [25]. This approach is similar to that performed by Metha et al. for the analysis of the oxygen defect model in $YBa_2Cu_3O_{6+y}$ [26]. Thus, the reference compound for the incorporation of oxygen excess using the Kröger–Vink notation is expressed by $(Sr'_{La})_2(Sr^x_{Sr})(Fe^x_{Fe})_2(O^x_O)_6V^{\bullet\bullet}_O$ where the replacement of two La by Sr generates two negative charges (Sr'_{La}), which are compensated by the created oxygen vacancy $V^{\bullet\bullet}_O$, Fe^x denotes a Fe^{+3} and, O^x_O is a

regular lattice oxygen ion. The crystal sites for the oxygen vacancy are not specified in this reference compound, but different empty crystallographic sites can be considered for the computation of the configurational entropy. Thus, in addition to the $O(1)$ crystallographic site indicated by a study of neutron powder diffraction (NPD) at room temperature [27], the presence of oxygen vacancies at high temperatures in the $O(2)$ and $O(3)$ sites may be also taken into account for the computation of the configurational entropy.

The proposed defect model equation for the oxygen incorporation disregarding the oxygen crystallographic site and considering localized charge carriers is expressed by the equation:

$$(Sr'_{La})_2(Sr^x_{Sr})(Fe^x_{Fe})_2(O^x_O)_6V^{\bullet\bullet}_O + \frac{\delta}{2}O_2 \leftrightarrow (Sr'_{La})_2(Sr^x_{Sr})(Fe^x_{Fe})_{2(1-\delta)}(Fe^{\bullet}_{Fe})_{2\delta}(O^x_O)_{6+\delta}(V^{\bullet\bullet}_O)_{1-\delta} \quad (5)$$

or the equivalent expression.

$$V^{\bullet\bullet}_O + \tfrac{1}{2}O_2 + 2Fe^x_{Fe} \leftrightarrow O^x_O + 2Fe^{\bullet}_{Fe}, \quad (6)$$

where $Fe^x_{Fe}/Fe^{\bullet}_{Fe}$ denotes the Fe^{+3}/Fe^{+4} redox couple.

The crystal site balance and the electroneutrality condition lead to the following expressions for the defect concentrations:

$$\begin{aligned}[Fe^x_{Fe}] &= 2(1-\delta)\\ [Fe^{\bullet}_{Fe}] &= 2\delta\\ [V^{\bullet\bullet}_O] &= 1-\delta\\ [O^x_O] &= n+\delta\end{aligned} \quad (7)$$

where n takes the value 0, 4 and 6 and "$n+\delta$" represents oxygen sites in the $O(1)$, $O(1)$ and $O(3)$, and $O(1)$, $O(2)$ and $O(3)$ crystal sites, respectively. In this approach, the oxygen vacancies are distributed with identical probability in the "$n+\delta$" available oxygen crystal sites.

The end member $(Sr'_{La})_2(Sr^x_{Sr})(Fe^x_{Fe})_2(O^x_O)_6V^{\bullet\bullet}_O$ is an oxygen acceptor and the oxygen excess is incorporated in the oxygen vacancies sites generating holes localized in the Fe^{+4} ions. The analysis of XPS data at room temperature of the $Sr_3Fe_2O_{6+\delta}$ compound [28] has confirmed that the electronic configuration of the Fe ions is mainly $3d^4(t^3_{2g}e^1_g)$. This defect model is similar to that used for describing the oxygen non-stoichiometry in the $La_{1-x}Sr_xFeO_{3-\delta}$ system [13,17].

The equilibrium reaction for the defect model, Eq. (6) leads to the following equation for the chemical potentials:

$$\tfrac{1}{2}\mu_{O_2} + (\mu_{V^{\bullet\bullet}_O} - \mu_{O^x_O}) + 2(\mu_{Fe^x_{Fe}} - \mu_{Fe^{\bullet}_{Fe}}) = 0. \quad (8)$$

The chemical potential for each defect species i is given by

$$\mu_i = \mu^0_i(T) + RT\ln a_i = \mu^0_i(T) + RT\ln\gamma_i[i], \quad (9)$$

where a_i is the activity, γ_i the activity coefficient and $[i]$ the concentration of i species. For an ideal solid solution the activity coefficients are $\gamma_i = 1$ and the activity is identical to the concentration $[i]$.

The substitution of Eqs. (7) and (9) in Eq. (8) leads to the next relationship between the oxygen chemical potential, the standard chemical potentials and the concentration of the defect species:

$$\begin{aligned}\mu_{O_2}(P,T) = 2\Big[&(\mu^0_{O^x_O}(T) - \mu^0_{V^{\bullet\bullet}_O}(T))\\ &+2(\mu^0_{Fe^{\bullet}_{Fe}}(T) - \mu^0_{Fe^x_{Fe}}(T))\Big]\\ &+2RT\ln\frac{\gamma_{O^x_O}\gamma^2_{Fe^{\bullet}_{Fe}}}{\gamma_{V^{\bullet\bullet}_O}\gamma^2_{Fe^x_{Fe}}}\\ &+2RT\ln\frac{[O^x_O][Fe^{\bullet}_{Fe}]^2}{[V^{\bullet\bullet}_O][Fe^x_{Fe}]^2}.\end{aligned} \quad (10)$$

From the comparison of Eq. (10) with Eq. (2), and in agreement with the regular solution model, we obtain for the partial molar enthalpy,

$$h_{O_2} = -2h^0_V - 4h^0_{Fe} + 2RT\ln\frac{\gamma_{O^x_O}\gamma^2_{Fe^{\bullet}_{Fe}}}{\gamma_{V^{\bullet\bullet}_O}\gamma^2_{Fe^x_{Fe}}}, \quad (11)$$

where $h^0_V = h^O_{V^{\bullet\bullet}_O} - h^0_{O^x_O}$ and $h^0_{Fe} = h^0_{Fe^x_{Fe}} - h^0_{Fe^{\bullet}_{Fe}}$ are the standard molar enthalpy of oxygen and electronic defects. The third term of Eq. (11) contains the deviation from the ideal solution due to defect interactions. The expression for s_{O_2} is given by

$$\begin{aligned}s_{O_2} &= -2s^0_V - 4s^0_{Fe} - 2R\ln\frac{[O^x_O][Fe^{\bullet}_{Fe}]^2}{[V^{\bullet\bullet}_O][Fe^x_{Fe}]^2}\\ &= -2s^0_V - 4s^0_{Fe} - 2R\ln\frac{(n+\delta)\delta^2}{(1-\delta)^3},\end{aligned} \quad (12)$$

where $s^0_V = s^0_{V^{\bullet\bullet}_O} - s^0_{O^x_O}$ and $s^0_{Fe} = s^0_{Fe^x_{Fe}} - s^0_{Fe^{\bullet}_{Fe}}$; s^0_{Fe} represents the difference in entropy between the $3d^5$ (Fe^{+3}) and $3d^4$(Fe^{+4}) states due to differences in degeneracy v of both magnetic states which gives a value of $s^0_{Fe} = -4.25\,Jmol^{-1}\,K^{-1}$ [14]. From the fitting of the experimental data with Eq. (12) and, using the value of s^0_{Fe} and $n=4$, we obtain for $s^0_V = -51\,Jmol^{-1}K^{-1}$. This value is close to those reported by Lankhorts et al. [14] for the $La_{0.6}Sr_{0.4}Co_{1-y}Fe_yO_{3-\delta}$ materials ($-45 < s^0_V < -35$).

The computation of the partial molar entropy strongly depends on the defect model considered. Thus, for itinerant charge carriers, the following expression is achieved:

$$s_{O_2} = -2s^0_V - 2R\ln\frac{[O^x_O]}{[V^{\bullet\bullet}_O]} = -2s^0_V - 2R\ln\frac{(n+\delta)}{(1-\delta)}. \quad (13)$$

On the other hand, if associated defects such as $(Fe^x_{Fe}\ldots V^{\bullet\bullet}_O\ldots Fe^x_{Fe})$ are taken into account, the partial

molar entropy is given by the following equation:

$$s_{O_2} = -2s^0_{Fe..V..Fe} + 2s^0_{O^x_0} + 4s^0_{Fe^\bullet_{Fe}} - 2R\ln\frac{[O^x_O][Fe^\bullet_{Fe}]^2}{[(Fe^x_{Fe}\ldots V^{\bullet\bullet}_O..Fe^x_{Fe})]} = -2s^0_{Fe..V..Fe} + 2s^0_{O^x_0} + 4s^0_{Fe^\bullet_{Fe}} - 2R\ln\frac{(n+\delta)\delta^2}{(1-\delta)}. \quad (14)$$

The experimental data of s_{O_2} have been fitted with Eqs. (12)–(14) and $n = 0, 4, 6$. In Fig. 4 we show the fitting of Eq. (12) with $n = 0$, 4 and 6 in addition to the fitting of Eqs. (13) and (14) with $n = 4$. No significant differences for the fitting of Eqs. (13) and (14) with $n = 0$, 4 and 6 were obtained. The fitting parameters are the standard molar entropy s^0_i for the different i species involved in each defect reaction. These parameters take different values depending on the defect equation and the n value. The best fitting is obtained with localized charges and oxygen vacancies random distributed with identical probability either in the $O(1)$ and $O(3)$ or all the oxygen sites $O(1)$, $O(2)$ and $O(3)$. It is clear that itinerant charge carriers give s_{O_2} values far from the experimental ones and other defects such as oxygen vacancies only in the $O(1)$ site or defect associations $(Fe^x_{Fe}\ldots V^{\bullet\bullet}_O\ldots Fe^x_{Fe})$ show a poor agreement. The existence of oxygen vacancies at the $O(3)$ oxygen site suggested from the fitting of the partial molar entropy should be in agreement with the presence of high ionic conductivity at high temperatures exhibited by this compound [10]. The jump of oxygen ions ($r(O^{2-}) = 1.4$ Å) through the oxygen lattice involving directly jumps along the route $O(1) \rightarrow O(1)'$ has a small probability due to the narrow spacing available between two adjacent Sr cations (~1 Å). Therefore, the high ionic conductivity necessarily involves the presence of empty oxygen sites in the $O(3)$ lattice position [29].

The dependence of the partial molar enthalpy with the oxygen content gives us an insight into the defect interactions. Thus, in agreement with Eq. (11) for an ideal solution ($\gamma_i = 1$) with localized charge carriers, the h_{O_2} is independent on the oxygen content [14]. A dependence of h_{O_2} with $6+\delta$ indicates a deviation from the ideal solution model. The data of Fig. 5 show a slight increase of h_{O_2} with increasing $6+\delta$ and therefore the presence of defect interactions for the $Sr_3Fe_2O_{6+\delta}$ material. The good fitting of the s_{O_2} data considering a random distribution of point defects suggests that the defect interaction are weak enough to prevent defect associations (clusters) or ordering. Consequently, the deviation of the ideal solution is evidenced only in the increases of h_{O_2} with δ. The dependence of h_{O_2} with "δ" within the experimental errors can be assumed as linear. This linear dependence is related to the activity coefficients through the next relationships:

$$RT\ln\frac{\gamma_{O^x_O}\gamma^2_{Fe^x_{Fe}}}{\gamma_{V^{\bullet\bullet}_O}\gamma^2_{Fe'_{Fe}}} = a\delta, \quad (15)$$

and

$$h_{O_2} = -2h^0_V - 4h^0_{Fe} + 2a\delta, \quad (16)$$

where the "a" parameter is obtained from the experimental data and is related to the defect interactions through the values of the activity coefficients γ_i. The average value for "a" obtained form the linear fitting of the data shown in Fig. 5 is $17 \pm 2\,kJ\,mol^{-2}$. This value thus computed only represents an average over the temperature range of measurements, since "a" depends on T. The h_{O_2} data give for $h^0_V + 2h^0_{Fe}$ a value of $= 74\,KJmol^{-1}$, which is considerably lower than those between 330 and $370\,KJmol^{-1}$ determined for the $La_{0.6}Sr_{0.4}Co_{1-y}Fe_yO_{3-\delta}$ system [14]. The "a" parameter is one order of magnitude lower than those obtained by Onuma et al. [25] for $La_{1-x}Ca_xCrO_{3-\delta}$. Onuma et al. [25] reports negative values of "a" ranging between -400 and $-250\,kJ\,mol^{-2}$. These negative values are due to the fact that in $La_{1-x}Ca_xCrO_{3-\delta}$ δ represent the concentration of oxygen vacancies, while our δ values indicate the concentration of extra oxygen in $Sr_3Fe_2O_6$. The low value of "a" obtained for $Sr_3Fe_2O_{6+\delta}$, suggests that the defect interactions are weaker than those determined for $La_{1-x}Ca_xCrO_{3-\delta}$. The increase of the partial molar enthalpy h_{O_2} with δ indicates that the mixing enthalpy "H_{mix}" between the two end compounds $Sr_3Fe_2O_6$ and $Sr_3Fe_2O_7$ is negative. Therefore, if $H_{mix} < 0$, $G_{mix} = H_{mix} - TS_{config} < 0$ at all temperatures and consequently the tendency to immiscibility is prevented.

3.3. Electrical conductivity

Fig. 6 shows the isotherms of the electrical conductivity as a function of pO_2. The slope of the log(σ) vs.

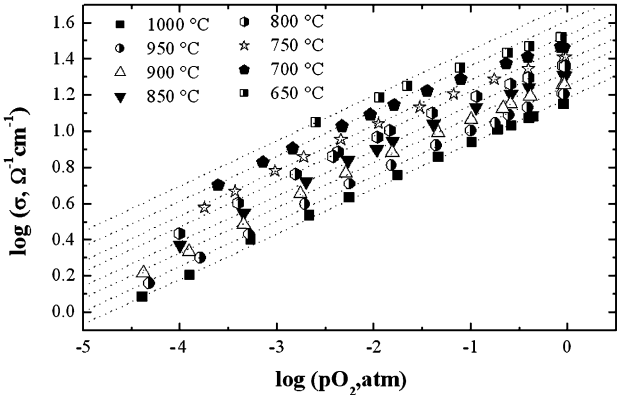

Fig. 6. Isotherms of the electrical conductivity as a function of log pO_2.

$\log(pO_2)$ curves is close to 1/4 at high temperatures and low pO_2 values. This slope decreases as pO_2 increases and T decreases. A positive slope corroborates the formation of electron hole p-type carriers (Fe^{+4}) and the value close to 1/4 confirms the presence of doubled oxygen charged vacancies $V_O^{\bullet\bullet}$ proposed in the defect Eq. (6). This behavior is similar to that recently measured by Patrakeev et al. [13] for $Sr_3Fe_2O_{6+\delta}$ and $pO_2 < 10^{-5}$ atm. who propose a conduction mechanism by small polarons.

The conductivity (σ_p) can be expressed by the following equation:

$$\sigma_p = N_p p e \mu_p = \frac{2}{V_{u.c.}} x_p e \mu_p, \tag{17}$$

where p is the concentration of p-type carriers, N_p is the volume concentration of Fe, x_p its molar fraction, e the electron charge, μ_p the mobility and, $V_{u.c.}$ is the unit cell volume. Since we assume that the carriers in $Sr_3Fe_2O_{6+\delta}$ are localized, and in agreement with Eq. (7) we have

$$x_p = [Fe_{Fe}^{\bullet}] = 2\delta. \tag{18}$$

A rough estimation for the mobility can be obtained from Eq. (17) assuming that it does not depend on $[V_O^{\bullet\bullet}]$. Thus, taking $V_{u.c.} = 301.8\,\text{Å}^3$ from XRD data at room temperature, we obtain values for the thermal activated mobility's ranging between $0.015 < \mu_p < 0.03\,cm^2\,V^{-1}\,s^{-1}$, for $0.2 < x_p < 1$. These values are close than those reported by Patrakeev et al for the same compound [13].

At high temperatures and low pO_2 where the carrier concentration is small, we can assume that the mobility μ_p is independent of the carrier's concentration (p). In this limit $[O_O^x] \approx 6$, $[V_O^{\bullet\bullet}] \approx 1$, $[Fe_{Fe}^x] \approx 2$, $[Fe_{Fe}^{\bullet}] = 2\delta$, and according to the mass action law $\sigma_p \propto [Fe_{Fe}^{\bullet}] \propto p_{O_2}^{1/4}$, which agrees with the high-temperature data shown in Fig. 6. At low T and high pO_2, the carrier concentration increases and the above condition is no more valid. Therefore, a deviation of the 1/4 slope should be expected as is shown in the data of Fig. 6. As the carrier concentration increases, another localized carrier may occupy the neighboring site. In this case the mobility is also a function of the carrier concentration due to site blocking [30] and in the frame of the small polaron theory within the non-adiabatic approximation in which the electron-transfer matrix element J is assumed to be much smaller than the lattice relaxation energy E_r [30], the mobility is given by

$$\mu_p = \frac{(1-x_p)ea^2J^2}{kT\hbar}\left[\frac{\pi}{4E_akT}\right]^{1/2}\exp\left(-\frac{E_a}{kT}\right), \tag{19}$$

where a is the hopping distance, e is the electron charge, T is the temperature, E_a is the small-polaron activation energy, related to E_r and, k and $\hbar$ are respectively the Boltzman and Planck constants.

Form Eqs. (17) and (19), the conductivity is expressed by

$$\sigma = \frac{2x_p(1-x_p)e^2a^2J^2}{V_{u.c.}k\hbar T}\left[\frac{\pi}{4E_akT}\right]^{1/2}\exp\left(-\frac{E_a}{kT}\right). \tag{20}$$

By combination of electrical conductivity and thermogravimetry data an experimental relation between σ and the carrier concentration (δ) can be established. This relation at different temperatures is shown in Fig. 7. It can be seen that for a given oxygen content value, the electrical conductivity increases as T increases, confirming the expected thermally activated behavior for the small polaron mechanism.

In Fig. 8 are presented the $\ln(\sigma T^{3/2})$ vs. $1/T$ data for different "$6+\delta$" values. For each value of "$6+\delta$" the $\ln(\sigma T^{3/2})$ vs. $1/T$ data show a linear behavior with a slope decreasing with increasing "$6+\delta$". In Fig. 9 are plotted the E_a vs. "$6+\delta$" values determined from the

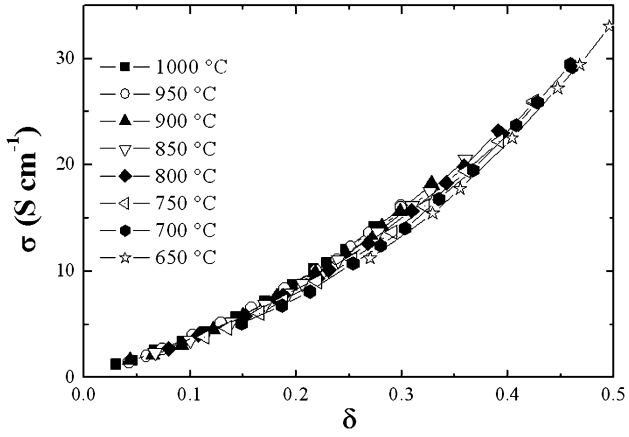

Fig. 7. Electrical conductivity "σ" as a function of "δ" at several temperatures.

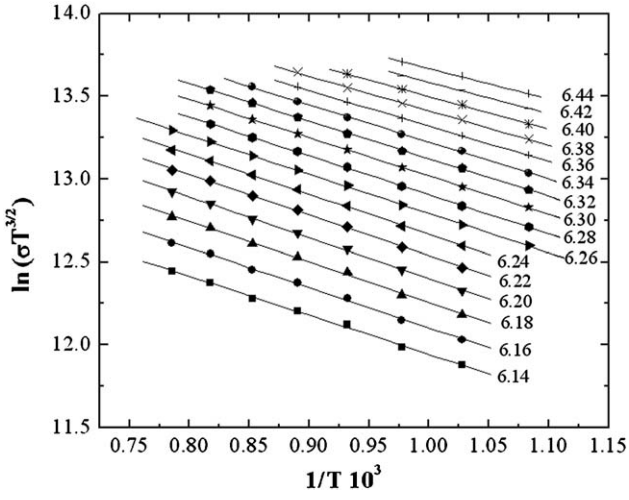

Fig. 8. $\ln(\sigma T^{3/2})$ vs. $1/T$ for $Sr_3Fe_2O_{6+\delta}$ at different oxygen contents.

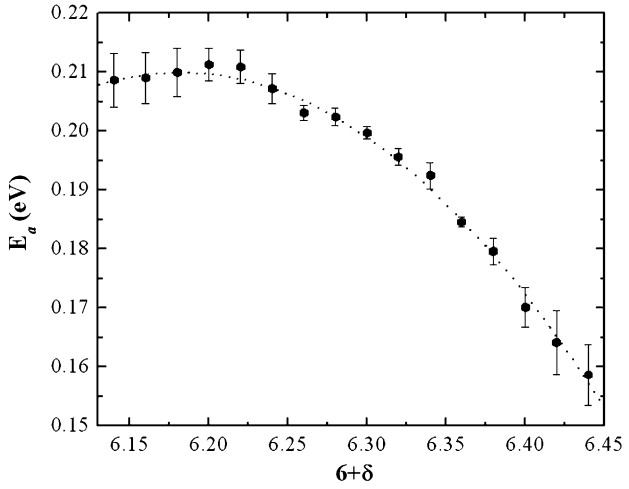

Fig. 9. Activation energy "E_a" as a function of "$6+\delta$". The solid line is a guide for the eye.

$\ln(\sigma T^{3/2})$ vs. $1/T$ slope within the interval $6.14 \leqslant 6+\delta \leqslant 6.44$.

The values of E_a for $6+\delta < 6.14$ are not shown since they present a high scatter mainly due to the errors in the pO_2 vs. $6+\delta$ determination close to $6+\delta \sim 6.00$. An appreciable dependence of E_a with "$6+\delta$" can be seen, which is consistent with the small polaron theory [31] and it is attributable to the overlap between the polarons clouds. This overlap is not negligible for high concentrations of polarons and therefore for small distance between them. An elementary electrostatic approach [31] predicts a dependence of the activation energy with the distance between polarons due to polarization effects of the type $(1/r_0 - 1/R)$, where r_0 is the radius of the polaron and R the distance between polarons. Thus, as R increases, the activation energy increases. An interesting feature of Fig. 9 is the observed saturation of E_a for $6+\delta < 6.20$ suggesting that the polaron clouds should not overlap for $6+\delta < 6.20$.

4. Conclusions

- The high-temperature thermodynamic measurements allow the determination of the partial molar entropy and enthalpy as a function of the oxygen content.
- We used a simple but rough approximation for computing the configurational entropy that is the assumption on identical probability for distributing the oxygen vacancies in the different oxygen crystal sites. In fact, the oxygen occupancy at the $O(1)$, $O(2)$ and $O(3)$ crystal sites should be quite different since the bonding energy for these sites must not be the same. However, our approach clearly suggests that oxygen vacancies at high temperatures are also present at $O(2)$ and $O(3)$ sites, in addition to those indicated by a NPD study at room temperature for $O(1)$ site.
- The partial molar enthalpy indicates a weak interaction between defects excluding any degree of defect associations (clusters) or ordering.
- The combination of the high-temperature thermodynamic data with resistivity measurements allows the determination of the dependence of the conductivity with temperature at fixed values of the oxygen content. The conductivity is thermally activated and is consistent with a small polaron type behavior.
- The set of thermodynamic and resistivity data confirm the defect model proposed for the $Sr_3Fe_2O_{6+\delta}$ material.

Acknowledgements

We gratefully acknowledge the help of V. Grünfeld in the English revision of this manuscript. This work was supported by CNEA (Argentine Research Commission), Fundación Antorchas (Argentina), Cooperation Program ECOS-SUD (Project A02E02) and ANPCyT (Agencia Nacional de Promoción Científica y Técnica Argentina) through PICT 02-12-12455 and PICT 12-14493.

The authors also acknowledge the help of Ing. N. Grunbaum for the technical assistance in this work.

Appendix A. Supplementary material

The online version of this article contains additional supplementary material. Please visit doi:10.1016/j.jssc.2005.06.010.

References

[1] S.J. Skinner, Int. J. Inorg. Mater. 3 (2001) 113.
[2] HJ. Bouwmeester, A.J. Burggraf, in: P.J. Gellings, H.J. Bouwmeester (Eds.), The CRC Handbook of Solid State Electrochemistry, CRC Press, Boca Raton, FL, 1997 (Chapter 14).
[3] A. Hammouche, A. Caneiro, E. Siebert, A. Hammou, M. Kleitz, J. Electrochem. Soc. 138 (1991) 1212.
[4] B. Gharbage, M. Henault, T. Pagnier, A. Hammou, Mater. Res. Bull. 26 (1991) 1001.
[5] J. Mizusaki, T. Matsuura, S. Yamauchi, K. Fueki, J. Tabuchi, J. Electrochem. Soc. 136 (1989) 2082.
[6] J. Mizusaki, Y. Mima, S. Yamauchi, K. Fueki, H. Tagawa, J. Solid State Chem. 80 (1989) 102.
[7] N. Grunbaum, L. Mogni, F. Prado, A. Caneiro, J. Solid. State Chem. 177 (2004) 2350.
[8] S. Pei, M.S. Kleefisch, T.P. Kobylinski, J. Faber, C.A. Udovich, V. Zhang-McCoy, B. Dabrowski, U. Balachandran, R.L. Mieville, R.B. Poeppel, Catal. Lett. 30 (1995) 201.
[9] T. Armstrong, F. Prado, A. Manthiram, Solid State Ionics 140 (2001) 89.
[10] F. Prado, T. Armstrong, A. Caneiro, A. Manthiram, J. Electrochem. Soc. 148 (2001) J7.

[11] A. Manthiram, F. Prado, T. Armstrong, Solid State Ionics 152–153 (2002) 647.
[12] K. Mori, T. Kamiyama, H. Kobayashi, S. Torii, F. Izumi, H. Asano, J. Phys. Chem. Solids 60 (1999) 1443.
[13] M.V. Patrakeev, I.A. Leonidov, V.L. Kozhevnikov, V.V. Kharton, Solid State Sci. 6 (2004) 907.
[14] M.H.R. Lankhorst, J.E. Ten Elshof, J. Solid State Chem. 130 (1997) 302.
[15] M.H.R. Lankhorst, H.J.M. Bouwmeester, H. Verjeij, J. Solid State Chem. 13 (1997) 555.
[16] J. Mizusaki, Y. Mima, S. Yamauchi, K. Fueki, J. Solid State Chem. 80 (1989) 102.
[17] J. Mizusaki, M. Yoshihiro, S. Yamauchi, K. Fueki, J. Solid State Chem. 58 (1985) 257.
[18] W. Sitte, E. Bucher, W. Preis, Solid State Ionics 154–155 (2002) 517.
[19] E. Bucher, W. Sitte, Solid State Ionics 173 (2004) 23.
[20] R.B. Mitberg, M.V. Patrakeev, I.A. Leonidov, V.L. Kozhevnikov, K.R. Poeppelmeier, Solid State Ionics 130 (2000) 325.
[21] A. Caneiro, P. Bavdaz, J. Fouletier, J.P. Abriata, Rev. Sci. Instrum. 53 (1982) 1072.
[22] A. Caneiro, M. Bonnat, J. Fouletier, J. Appl. Electrochem. 11 (1981) 83.
[23] IUPAC, Commission on Thermodynamics, Oxygen, International Thermodynamics Tables of the Fluid State-9, Blackwell Sci., Oxford, 1987.
[24] S. Onuma, K. Yashiro, S. Miyoshi, A. Kaimai, H. Matsumoto, Y. Nigara, T. Kawada, J. Mizusaki, K. Kawamura, N. Sakai, H. Yokokawa, Solid State Ionics 174 (2004) 287.
[25] D. Samaras, A. Collomb, J.C. Joubert, Mater. Res. Bull. 9 (1974) 693.
[26] A. Metha, D.M. Smyth, Phys. Rev. B 51 (1995) 15382.
[27] S.E. Dann, M.T. Weller, D.B. Curie, J. Solid State Chem. 97 (1992) 179.
[28] M. Abbatte, H. Ascolani, L. Mogni, F. Prado, A. Caneiro, Physica B 354 (2004) 7.
[29] Y.A. Shilova, M.V. Patrakeev, E.B. Mitberg, I.A. Leonidov, V.L. Kozhevnikov, K.R. Poeppelmeier, J. Solid State Chem. 168 (2002) 275.
[30] R. Raffaelle, H.U. Anderson, D.M. Sparkin, P.E. Parris, Phys. Rev. B 43 (1991) 7991.
[31] Mott, J. Non-Cryst. Solid 1 (1968) 1.